J Solid State Electrochem (2007) 11:1541–1548
DOI 10.1007/s10008-007-0350-0

ORIGINAL PAPER

Electrocatalysis of oxygen reduction and hydrogen oxidation in platinum dispersed on tungsten carbide in acid medium

L. G. R. A. Santos · K. S. Freitas · E. A. Ticianelli

Received: 7 February 2007 / Revised: 9 April 2007 / Accepted: 2 May 2007 / Published online: 23 May 2007

Abstract Tungsten carbide dispersed on a high surface area carbon (W_2C/C) prepared by a sonochemical method was used as the support of a Pt-based electrocatalyst (Pt-W_2C/C). The resulting materials were tested for two important reactions with practical interest in fuel cells, that is, the oxygen reduction and hydrogen oxidation reactions, in acid medium. The electrochemical techniques considered were cyclic voltammetry, linear sweep voltammetry, and steady-state polarization curves, obtained utilizing an ultrathin catalyst layer in a rotating ring–disk electrode. The results showed that the Pt-W_2C/C catalyst led to a remarkable enhancement of the oxygen reduction in acid medium, when compared to the standard Pt/C, both following a four-electron mechanism. The hydrogen oxidation reaction showed similar kinetics on Pt-W_2C/C and Pt/C following the direct discharge mechanism on both catalysts. The W_2C/C support presented remarkable activity for the hydrogen oxidation reaction, most probably after the Heyrovsky–Volmer mechanism at low overpotential and the direct discharge irreversible mechanism at high overpotentials.

Keywords Tungsten carbide · Oxygen reduction · Hydrogen oxidation

Dedicated to the memory of Francisco C. Nart

L. G. R. A. Santos · K. S. Freitas · E. A. Ticianelli (✉)
Instituto de Química de São Carlos, USP,
C. P. 780, São Carlos, SP 13560-970, Brazil
e-mail: edsont@iqsc.usp.br

Introduction

Fuel cells are attractive power sources for both stationary and electric vehicle applications due to their high energy conversion efficiencies and low pollutant emissions. Among the various types of fuel cells, the proton exchange membrane fuel cell (PEMFC) and the direct methanol fuel cell (DMFC) are very promising. However, their large-scale production and commercialization are confronted with various issues including the cost of the Pt-based electrocatalysts, the poisoning of the electrocatalysts by small amount of impurities, low activity of the fuel cell when the anode uses liquid fuels (methanol, ethanol, etc.), and the poor intrinsic kinetics of the cathodic oxygen reduction reaction (ORR).

While the overpotential for the anodic oxidation of pure hydrogen is negligible even at high current densities due to the very facile H_2 oxidation kinetics on platinum, it shows a strong kinetic inhibition due to CO poisoning when the anode uses methanol or reformed hydrogen gas [1]. Because of this, a good anode catalyst for PEM fuel cells has to show not only high catalytic activity towards hydrogen oxidation but also tolerance for CO [2–5]. It is also known that the cell voltage of both PEMFC and DMFC, independently of the fuel, is limited by the slow reaction kinetics at the oxygen electrode [6].

Platinum supported on high surface area carbon substrates is still the most widely used electrocatalyst in the fuel cell, both at the anode and the cathode [7]. With the objective of lowering the cost, other electrocatalysts, such as metal oxides [8], metal porphyrins [9, 10], and metal carbides [11], have been investigated over the years. Another way to lower the cost is the alloying of platinum with other less expensive transition metals.

Recently, tungsten carbides have been examined as heterogeneous catalysts because their activity is often similar to that of the platinum group metals [12–15]. Tungsten carbides show interesting chemical and/or electrochemical activities in a great quantity of reactions [16] including those occurring in the PEMFC [17] and DMFC [18]. Preparation of nanoscaled tungsten carbides by different methods was recently reported, including tungsten carbide nano wires [16]. Synergistic effects have been evidenced by the addition of tungsten carbides into metal or oxide composites. For example, the composite of Pt/C and tungsten carbide showed promising activities for oxygen reduction in both alkaline and acid media [19].

This study aims to evaluate the performance of a platinum catalyst supported in tungsten carbides (Pt-W_2C/C), prepared by the sonochemical method, for two reactions for application in fuel cells, that is, the oxygen reduction reaction and hydrogen oxidation reaction, in acid medium. The electrochemical techniques considered in the study were cyclic voltammetry, chronoamperometry, linear sweep voltammetry, and steady-state polarization curves, obtained utilizing an ultrathin layer in a rotating ring–disk electrode (RRDE).

Experimental

Preparation of tungsten carbide

The procedure to prepare the tungsten carbide was the same as that reported previously in the literature [15]. A slurry of tungsten hexacarbonyl (1 g in 50 ml of hexadecane) and an appropriate amount of carbon powder (Vulcan XC-72R) was sonicated with a high-intensity ultrasonic bath (Unique, 0.5 in Ti horn, 19 kHz, 80 W cm^{-2}) at 90 °C for 3 h under argon to yield a completely black powder slurry. The solution was filtered, washed several times with purified degassed pentane, and heated at 100 °C. Since the presence of oxygen oxide could affect the catalytic activity, it was removed before catalytic studies by heating in a flowing 1:1 CH_4/H_2 mixture at 300 °C for 1 h, then at 400 °C for 1 h, and finally at 500 °C for 12 h [15]. After this carburization, excess of carbon, hydrogen, and oxygen had been largely removed.

Preparation of the tungsten carbide supported Pt electrocatalyst

A solution was prepared by mixing chloroplatinic acid (H_2PtCl_6), water, and W_2C/C previously prepared. The solution was treated in an ultrasonic bath to form uniformly dispersed ink. The solution was kept at 80 °C, and the platinum was then reduced with a formic acid solution [20], which was slowly added under stirring. The solution was filtered, and the powder washed several times with purified water and dried at 80 °C for 1 h.

Characterization

The atomic ratios of the Pt-W_2C/C, Pt/C, and W_2C/C electrocatalysts were obtained by EDX (energy dispersive X-ray) analysis in a scanning electron microscope (DSM 960 Zeiss) provided with a microanalyzer Link Analytical QX 2000 and a SiLi detector using a 20 KeV electron Beam. X-ray diffraction (XRD) were obtained using a Rigaku Rotaflex Mod. RU-200B equipment with Cu Kα radiation (λ=0.15406) generated at 40 kV and 20 mA. Scans were done at 2° min^{-1} for 2θ values in the range of 20 and 100°. To estimate the particle size, the Scherrer's equation [21] was used. For this purpose, the (220) peak of the Pt face-centered cubic (fcc) structure at 2θ=68° was selected. To improve the fitting quality of this peak, the XRD records for 2θ values from 60 to 80° were done at 0.02° min^{-1}.

Electrochemical cell and electrode preparation

A conventional one-compartment glass cell with a Luggin capillary was used in the electrochemical experiments. A large area platinized platinum foil served as the counter electrode and a reversible hydrogen electrode (RHE) system was used as the reference electrode. All the experiments were carried out in 0.5 mol l^{-1} H_2SO_4, prepared from high purity reagents (Mallinckrodt) and water purified in a Milli-Q (Millipore) system. The electrolyte was saturated with pure N_2, H_2, or O_2 gases, depending on the experiment. After preparation, the electrodes were immersed in oxygen-free electrolyte solutions at room temperature and cycled several times between 0.05 and 1.1 V at 50 mV/s until a steady-state voltammogram was reached. Cyclic voltammetry was used to characterize the electrocatalyst surface and to obtain the electrochemical active area. The platinum active surface area was estimated by obtaining the charge of hydrogen desorption in the potentials range from 0.05 to ~0.4 V vs RHE and assuming that hydrogen is only adsorbed on Pt sites with 210 μC corresponding to 1 cm^{-2} of exposed area. The double-layer charging currents were subtracted from the total voltammetric currents for obtaining the H desorption charge. All electrochemical experiments were conducted at room temperature (25±1 °C).

In all cases, the working electrodes were deposited as an ultrathin layer over a pyrolitic graphite disk (polished to a mirror finish before each experiment, 0.196 cm^2) of a RRDE. The working electrodes were prepared with 14 μg catalysts cm^{-2} (Pt/C, Pt-W_2C/C, or W_2C/C). A diluted Nafion solution (5 wt%, DuPont) was pipeted on the

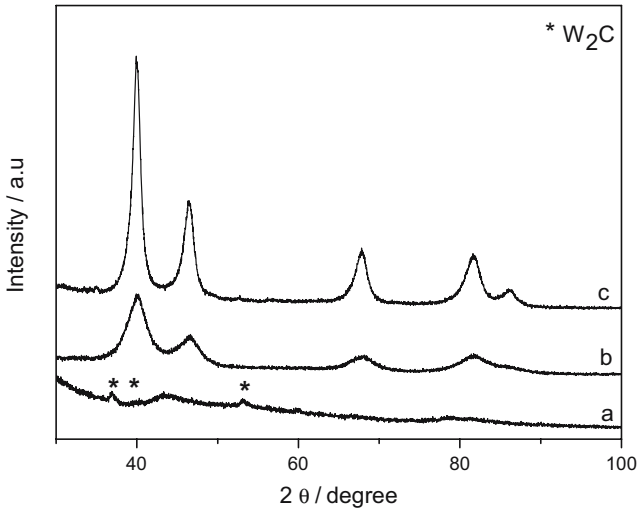

Fig. 1 XRD patterns for W_2C/C (*a*), Pt-W_2C/C (*b*), and Pt/C (*c*). *Asterisk* W_2C peaks

electrode surface to attach the catalyst particles onto the glassy carbon [22].

ORR measurements

Steady-state polarization curves were obtained with the RRDE at several rotation speeds to evaluate the ORR kinetic parameters, and the experiments were recorded in the potential range between 0.2 and 1.10 V vs RHE using an AUTOLAB bipotentiostat (PGSTAT30). In this system, the ring electrode (platinum) was used to sensor the H_2O_2 produced in the working disk electrode. This was made by measuring the magnitude of the H_2O_2 oxidation current at a constant potential of 1.2 V vs RHE, where the oxygen reduction and evolution currents are negligible, and the oxidation of peroxide is diffusion limited. The collection efficiency, *N*, was determined for the RRDE electrode, from the slope of an I_R vs I_D plot at different rotation rates, using

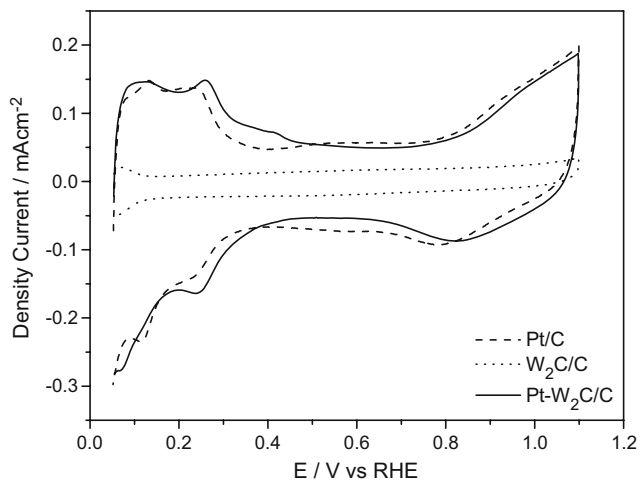

Fig. 2 Cyclic voltammograms obtained for W_2C/C, Pt-W_2C/C, and Pt/C in 0.5 mol l^{-1} H_2SO_4 at 50 mV s^{-1}

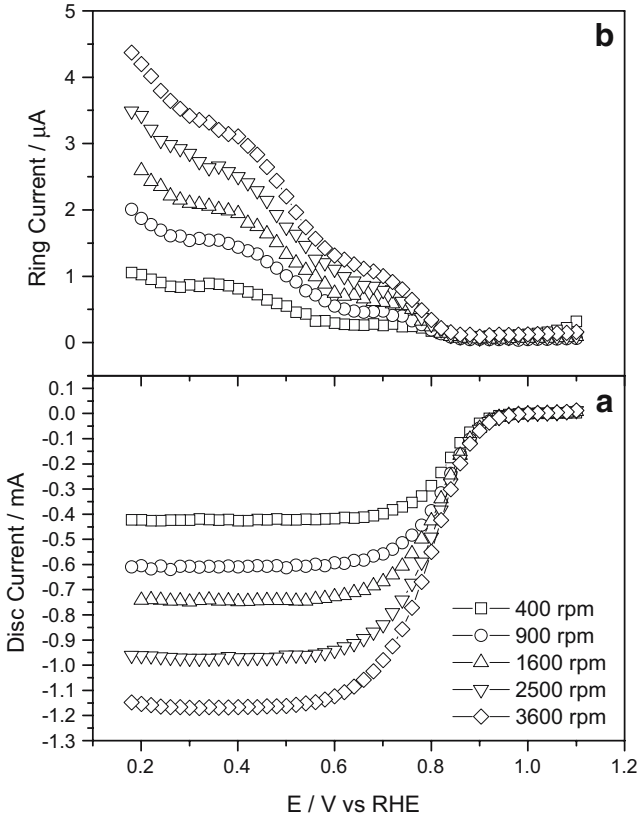

Fig. 3 Steady-state polarization curves for the ORR on the Pt-W_2C/C catalyst in 0.5 mol l^{-1} H_2SO_4 at several rotate speeds. **a** Disc current, **b** ring current (E_r=1.2 V)

an electrolyte solution 10^{-2} mol l^{-1} of $K_3Fe(CN)_6$ in 0.5 mol l^{-1} H_2SO_4. A value of *N* equal to 0.36 was found. This value was used to determine the peroxide formation and the number of electrons in the ORR.

Hydrogen oxidation

Polarization curves for the hydrogen oxidation were obtained at 2 mV s^{-1} using the RRDE at several rotation speeds to evaluate the hydrogen oxidation reaction kinetic parameters. The experiments were recorded in the potentials range between 0 and 0.6 V, also using the AUTOLAB PGSTAT30 bipotentiostat.

Results and discussion

Characterization

The composition of the W_2C/C support was determined by EDX analysis. The nominal mass ratio of W to C was 40%, but it was found that the mass ratio of W to C in the final product was approximately 10%. EDX was also used to determine the amount of platinum in the Pt-W_2C/C, and

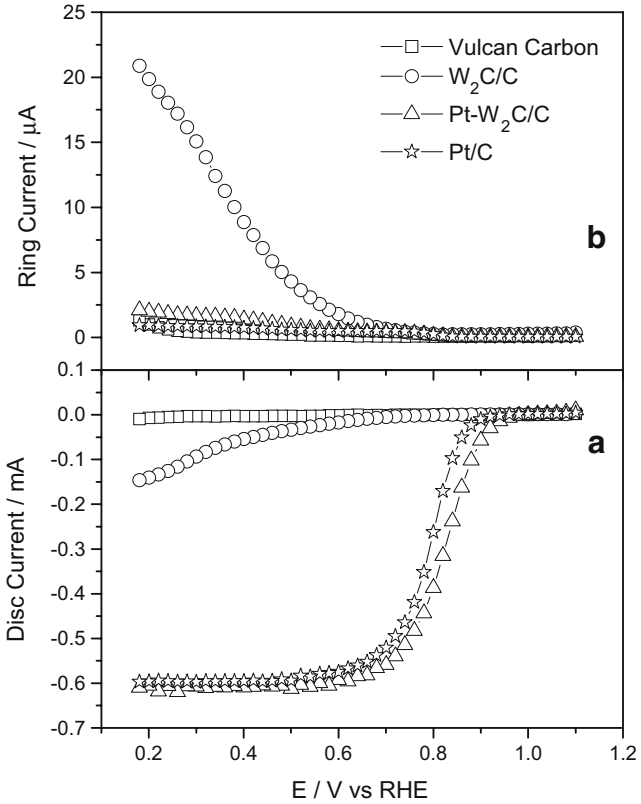

Fig. 4 Steady-state polarization curves for the ORR on W_2C/C, Pt-W_2C/C, and Pt/C in 0.5 mol l^{-1} H_2SO_4 at 900 rpm. **a** Disc current, **b** ring current (E_r=1.2 V)

this resulted to 21 wt%, which is very close to the nominal value (20 wt%). The amount of Pt in Pt/C was also the same as the nominal value, 20 wt%.

The catalysts were analyzed by XRD, as shown in Fig. 1. The XRD pattern confirmed that the tungsten carbide prepared here is in the form of nanocrystals. The peaks observed in the diffractogram are identified as those for pure W_2C. Meng and Shen [23] also obtained pure W_2C, using the intermittent microwave heating method, but they also noted the presence of WC when the amount of W was high, that is, when the atomic ratio of W to C was 40%. The low intensity sign for the XRD patterns for the W_2C/C may be due to the low content of W_2C compared to that of carbon. Curves b and c show the XRD patterns for the Pt-W_2C/C and for a commercial Pt/C catalyst, respectively. It is clear that the XRD pattern of Pt-W_2C/C combines the crystalline features of Pt and W_2C. The broad reflections of both Pt catalysts indicate that they are nanostructured materials with small grain size. In accordance to this, the average crystallite sizes calculated from Scherrer's equation [21] for the Pt-W_2C/C and Pt/C catalysts resulted to 5.4 and 2.6 nm, respectively.

Electrochemical measurements

Cyclic voltammetric profiles for Pt-W_2C/C and Pt/C with the current normalized by the real Pt surface area (see above) and for W_2C/C are presented in Fig. 2. The results show the typical behavior regarding the hydrogen and the oxide regions for carbon-supported Pt in acid solutions [24–26]. The peaks for the H_{upd} region for the Pt-W_2C/C are well resolved and very similar to that of the Pt/C catalyst. A small difference has been found in the potential near 410 mV, where a small oxidation peak is observed. This feature is surely related to redox processes involving Pt-WO_x composites [27], which were not detected by XRD because it may be presented at a small amount or as an amorphous phase. Other possibility is that the tungsten oxide was formed when the catalyst was placed in contact with the acid solution. For W_2C/C, no redox peaks were observed in this region of potential in acid solution under ambient temperature [28].

In Fig. 2, a shift to higher potentials of the platinum oxide reduction peak was observed for the Pt-W_2C/C, compared to Pt/C. Such an anodic shift can be attributed to a decrease in the desorption free energy (ΔG_{ads}) of Pt–OH and Pt–O. This means that the adsorption strength of adsorbed oxygen species on Pt-W_2C/C is lower than on Pt/C, and so, the reduction in intermediates containing oxygen is more facile. In the presented work, no changes in the shape or size of the voltammograms were observed during the whole period of measurements for all catalysts, indicating the large stability of the materials.

ORR results

Figure 3 shows steady-state polarization curves for the ORR in the disk and the currents for H_2O_2 oxidation in the

Table 1 Tafel coefficients (b), number of electrons (n), and percentage of peroxide formation (%H_2O_2) at several electrode potentials (E) for the Pt-W_2C/C and Pt/C catalysts where l_η (low overpotential region) and h_η (high overpotential region)

Catalysts	n (E=0.88 V)	n (E=0.70V)	n (E=0.3V)	%H_2O_2 (E=0.88V)	%H_2O_2 (E=0.7V)	%H_2O_2 (E=0.3V)	b (l_η)mV decade^{-1}	b (h_η)mV decade^{-1}
Pt/C	3.98	3.99	3.95	0.11	0.34	1.6	58	130
Pt-W_2C/C	3.99	3.99	3.97	0.29	0.5	1.51	66	123
W_2C/C	–	2.96	2.76	–	0.52	0.62	–	–

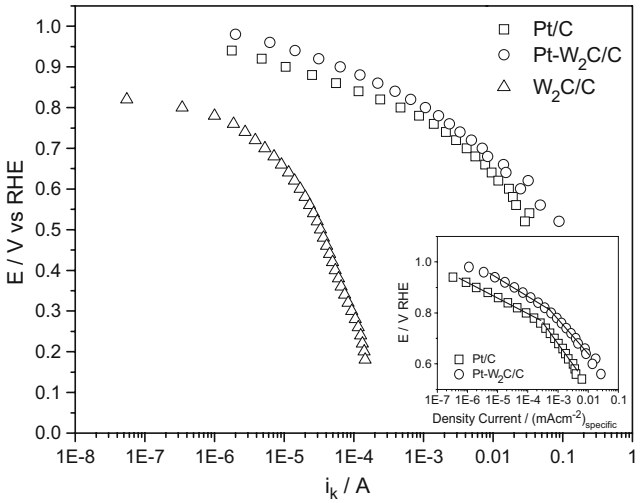

Fig. 5 Mass-transport-corrected Tafel plots for the ORR on the Pt-W_2C/C, W_2C/C, and Pt/C materials in 0.5 mol l^{-1} H_2SO_4 at 25 °C. *Inset* mass-transport Tafel plots for the Pt-W_2C/C and Pt/C with currents normalized per unit of Pt surface area

ring, for the Pt-W_2C/C catalyst, at several rotation speeds. From these results, it is observed that the ORR is diffusion-controlled when the potential is more negative than 0.6 V and is under mixed kinetic–diffusion control in the potential region between 0.6 and 0.9 V. The steady-state polarization curves for different materials at 900 rpm are compared in Fig. 4. From these results, it is clearly noted that the Vulcan carbon is not active, while W_2C/C is very little active for the ORR in acid medium. It is also noted that the ORR limiting currents for the Pt-W_2C/C assume values close to those for the Pt/C catalyst, both showing low ring current signals for peroxide oxidation.

Results also show that in the activation and kinetic–diffusion controlled regions, a higher activity is observed for the Pt-W_2C/C material compared to the Pt/C. Due to the very low activity for ORR in the W_2C/C and the smaller surface area of Pt in Pt-W_2C/C when compared with Pt/C (2.2 and 5.4 cm^{-2}, respectively), the enhancement of the ORR kinetics in the Pt-W_2C/C may be attributed to changes on the platinum electronic states caused by the presence of tungsten carbide (see below).

The number of electrons per oxygen molecule (n) and the relative amount of H_2O_2 (%H_2O_2) were obtained by the equations [29, 30]:

$$n = \left(\frac{{}^{4}I_D}{I_D + \frac{I_R}{N}}\right) \quad ;\%H_2O_2 = \left(\frac{\frac{2I_R}{N}}{I_D + \frac{I_R}{N}}\right) \tag{1}$$

where N is the collection efficiency of the ring, I_D is the disc current, and I_R is the ring current. These results are reported in Table 1 for all catalysts, for E=0.88, 0.7, and 0.3 V. Results show that the values of n are close to 4 for both Pt-containing catalysts, in agreement with the very small peroxide oxidation currents observed in Figs. 3 and 4. A considerably lower value of n was obtained for W_2C/C. These results also confirm the very low formation of H_2O_2 for the Pt-based catalyst under the present experimental conditions. On the other hand, much higher H_2O_2 formation is seen for W_2C/C.

The electrocatalytic activity for the ORR on these electrocatalysts was compared through mass-transport-corrected Tafel plots as shown for the Pt-W_2C/C and Pt/C in Fig. 5. Because diffusion limitations were not apparent for W_2C/C in this case, there is no need to correct for mass transport. In the insert are the results for the Pt-based catalysts with the currents normalized by real Pt surface area evaluated by cyclic voltammetry. The values of the Tafel slopes obtained from these lines are included in Table 1. Similar Tafel behaviors were obtained for other kinds of Pt-W_2C/C and Pt-based catalysts, as also shown in previous works [6, 21, 22, 31]. Two different linear regions are

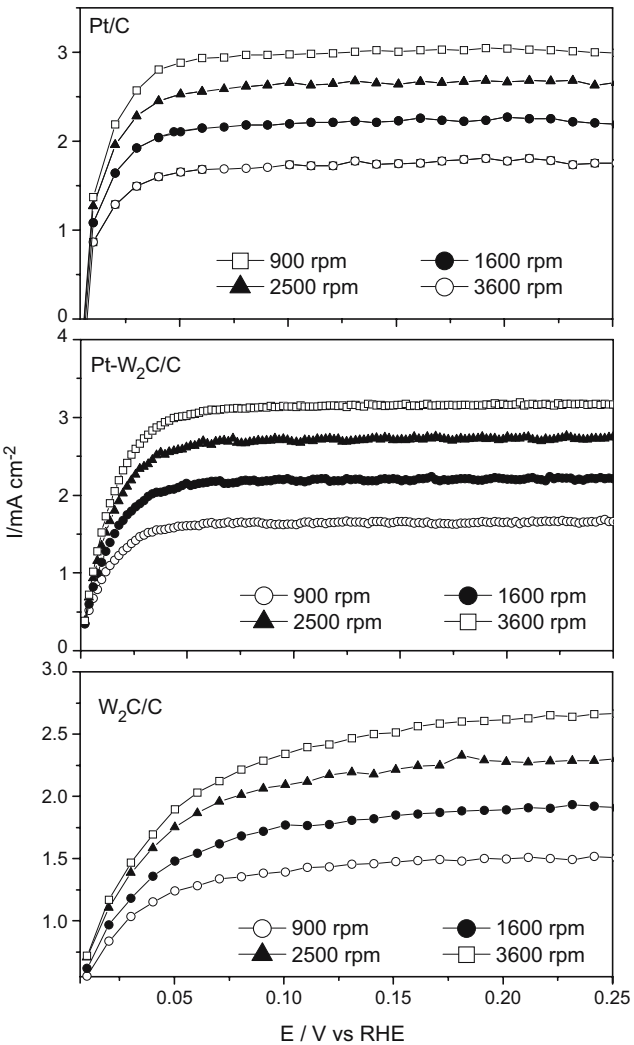

Fig. 6 Steady-state current–potential plots for the oxidation of hydrogen at several rotation rates, in 0.5 mol l^{-1} H_2SO_4 at 25 °C

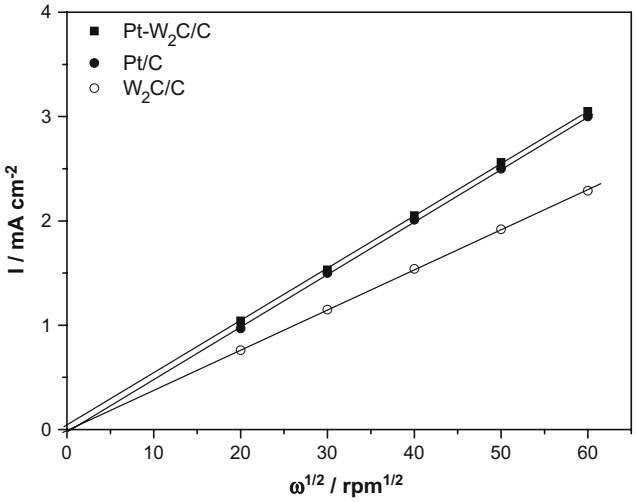

Fig. 7 Levich diagrams for the hydrogen oxidation on the Pt-W_2C/C, W_2C/C, and Pt/C catalysts, in 0.5 mol l^{-1} H_2SO_4

observed, with slopes close to 60 mV $decade^{-1}$ for low overpotential (l_η) and 120 mV $decade^{-1}$ for high overpotentials (h_η), in agreement to previous results for Pt/C [6, 29]. This behavior has been explained in terms of the coverage of adsorbed oxygen, which follows a Temkin istotherm at low overpotential (the surface has high coverage of oxides and/or adsorbed oxygen intermediates) and a Langmuir isotherm at high overpotentials (the surface has low coverage of oxides and/or adsorbed oxygen intermediates).

From the inset in Fig. 5, it is clearly concluded that Pt-W_2C/C present considerably higher specific activity compared to Pt/C. Assuming that the reaction occurs only on the Pt atoms, two previously reported mechanisms could be used to discuss the increase in the ORR kinetics on the Pt atoms in the Pt-W_2C/C material. One hypothesis [32] assumes that an increase in the ORR kinetics may be assigned to a decrease in the Pt 5d band occupancy, which may result in a stronger interaction of adsorbed O_2 with Pt, decreasing the difficulty of breaking the O–O bond. On the contrary, following another model [33], the increase in the ORR kinetics would be assigned to a decrease in the Pt 5d band occupancy, meaning that the adsorption strength of adsorbed oxygen species decrease, and so, the reduction in intermediates containing oxygen adsorbed on the Pt surface becomes more facile. This last effect is confirmed by the results in Fig. 2, where it is clearly observed that the reduction in adsorbed oxygen intermediates on Pt is more facile in the presence of W_2C/C.

Oxidation of pure hydrogen

Figure 6 shows the steady-state current–potential curves for the hydrogen oxidation at 2 mV s^{-1} on the Pt/C, Pt-W_2C/C, and W_2C/C materials in 0.5 mol l^{-1} H_2SO_4, for various rotations rates. At low potentials, the currents are controlled by activation, but with the potential increase, mass transport starts to influence the current until a limiting value is reached above about 0.03 V, particularly for the Pt-based catalysts. Although smaller than for the Pt-based catalysts, considerable activity for the hydrogen oxidation reaction was observed for W_2C/C. Assuming laminar flow, the mass transport rate and, consequently, the limiting diffusional current can be described by the Levich equation [34]:

$$i_d = 0.62nFAD^{2/3}\nu^{-1/6}C^*\omega^{1/2} \quad (2)$$

where A is the geometric area of the electrode, D the diffusion coefficient, and C^* the solubility of the hydrogen in the electrolyte, ν the kinematics viscosity of the electrolyte, and ω is the rotation speed. Figure 7 displays the Levich plots for the oxidation of hydrogen, where the near-zero intercepts and the linear behavior indicate that the currents at the positive potential limit are essentially diffusion limited. The small differences of the slopes of the lines must be related to small differences of the geometric area of the active layer.

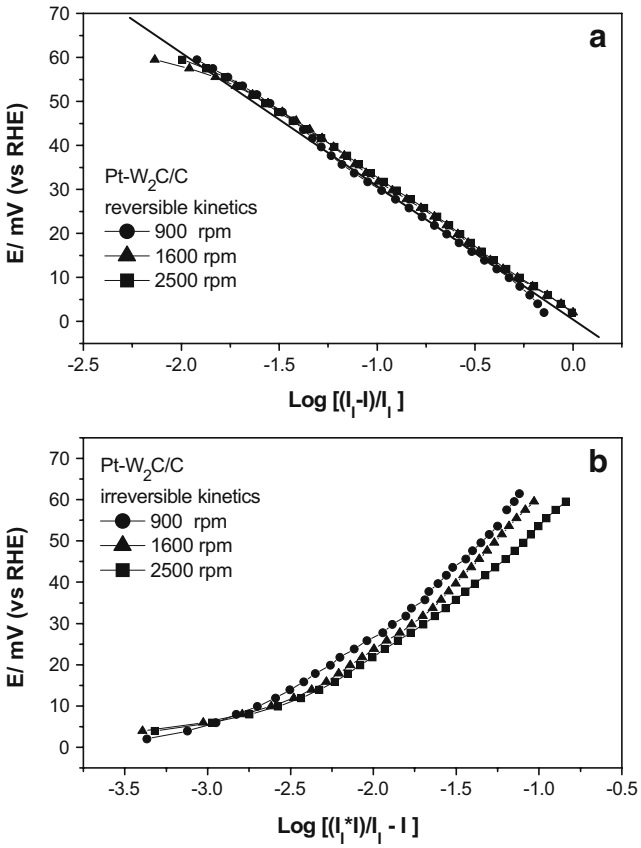

Fig. 8 (**a**) Mass-transport-corrected Tafel plots assuming reversible kinetics for the hydrogen oxidation on Pt-W_2C/C. (**b**) Mass-transport-corrected Tafel plots assuming irreversible kinetics for the hydrogen oxidation on Pt-W_2C/C

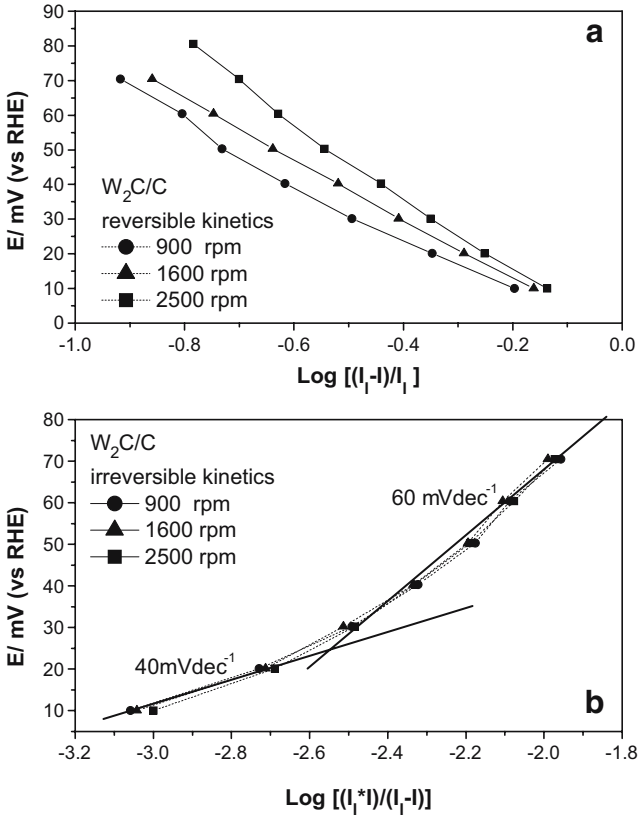

Fig. 9 (**a**) Mass-transport-corrected Tafel plots assuming reversible kinetics for the hydrogen oxidation on W_2C/C. (**b**) Mass-transport-corrected Tafel plots assuming irreversible kinetics for the hydrogen oxidation on W_2C/C

As in the case of the ORR, the kinetics and mechanism of the hydrogen oxidation reaction can be discussed by using mass-transport-corrected Tafel plots. Considering that the reaction is reversible,

$$H_2 \underset{\overleftarrow{k}}{\overset{\vec{k}}{\rightleftarrows}} 2H^+ + 2e^- \tag{3}$$

the kinetic equation for describing the electrode polarization can be written as [35]:

$$E = E^{o} - 2.303\frac{RT}{nF}\log\left(\frac{I_L^a - I}{I_L^a}\right) \tag{4}$$

where E is the electrode potential, E^o is the equilibrium potential of the reaction, I_L^a is the limiting anodic current and $2.303RT/nF$ is the Tafel slope. On the other hand, for an irreversible process, the equation is [35]:

$$E = E^{o} + b.\log\left(\frac{I \times I_L^a}{I_L^a - I}\right) - b.\log C_R^{\infty} - \text{constant} \tag{5}$$

where b is the Tafel slope for the hydrogen oxidation reaction, and C_R^{∞} is the solubility of the reagent in the liquid electrolyte.

Figures 8 and 9 show the Tafel plots for the H_2 oxidation at different rotation speeds for the Pt-W_2C/C and W_2C/C catalysts, assuming that the reaction follows the direct reversible or irreversible mechanisms [36–38]. Because the current rises very sharply reaching the limiting value, only the values between 0 and 0.08 V (vs RHE) could be used. The results for Pt/C presented essentially the same behaviors as those shown in the Fig. 8.

Comparing the plots of Fig. 8a and b, it is observed that, for Pt-W_2C/C, the result follows the prediction of Eq. 4 (reversible reaction) independently of the rotation rate. The same behavior was found for Pt/C. These results indicate that the hydrogen oxidation reaction follows the direct reversible mechanism in both Pt-based catalysts, in agreement with what is observed for a smooth Pt electrode [35]. The values of the Tafel coefficient for both materials are very close to 30 mV decade^{-1}, and so also in agreement with the reversible direct discharge [36–38] mechanism for T=25 °C.

The Tafel plots for the W_2C/C support shown in Fig. 9a and b confirmed that this catalyst presents considerable activity for the hydrogen oxidation reaction, but in this case, following the prediction of Eq. 5, is valid for an irreversible reaction. However, there was no linearity on the Tafel lines, which showed a Tafel slope close to 40 mV decade^{-1} at low overpotentials and 60 mV decade^{-1} at higher overpotentials. A value of 40 mV decade^{-1} corresponds to the theoretical prediction for the Heyrovsky/Volmer [36] mechanism, having Volmer as the rate-determining steps and with the catalyst surface presenting low degree of coverage of adsorbed hydrogen atoms [35]. On the other hand, at high overpotentials, the value of 60 mV decade^{-1} is consistent with the direct discharge irreversible mechanism [36], which is similar to the reversible case (Eq. 3), but having smaller rate constants. Further investigations are on course, including single-cell PEMFC measurements, to better characterize the hydrogen oxidation process in this material.

Conclusion

Tungsten carbide with and without Pt nanocrystals, prepared by a sonochemical method was tested for two important reactions with practical interest in fuel cell. A shift to higher potentials of the platinum oxide reduction peak was observed for the Pt-W_2C/C, compared to Pt/C. Such an anodic shift was attributed to a decrease in the desorption free energy (ΔG_{ads}) of Pt–OH and Pt–O, meaning that the adsorption strength of adsorbed oxygen species on Pt-W_2C/C is lower than on Pt/C. The results showed that Pt-W_2C/C leads to a remarkable enhancement of the ORR kinetics in acid medium, and this was attributed

to the fact that the electroreduction in the oxygenated intermediates is more facile.

The kinetics of the hydrogen oxidation reaction is similar on the Pt/C and Pt-W_2C/C catalysts, and the Tafel slopes obtained are in agreement with the direct discharge reversible mechanism. The W_2C/C support presented considerable activity for the hydrogen oxidation reaction, which more probably follows the Heyrovsky/Volmer mechanism at low overpotentials and the direct discharge irreversible mechanism at high overpotentials.

Acknowledgement The authors thank Fundação de Amparo a Pesquisa de São Paulo (FAPESP) and Conselho Nacional de Desenvolvimento Científico e Tecnológico (CNPq) for the financial support.

References

1. Samjeské G, Wang H, Löffler T, Baltruschat H (2002) Electrochim Acta 47:3681
2. Luna AMC, Câmara GA, Paganin VA, Ticianelli EA, Gonzalez ER (2000) Electrochem Commun 2:222
3. Câmara GA, Giz MJ, Paganin VA, Ticianelli EA (2002) J Electroanal Chem 537:21
4. Santiago EI, Camara GA, Ticianelli EA (2003) Electrochim Acta 48:3527
5. Santiago EI, Giz MJ, Ticianelli EA (2003) J Solid State Electrochem 7:607
6. Adzic RR (1998) Recent advances in the kinetics of oxygen reduction. In: Lipkowski J, Ross PN (ed) Electrocatalysis, chap 5. Wiley-VCH, New York
7. Gottesfeld S, Zawodzinski TA (1997) In: Alkire RC, Gerischer H, Kolb DM, Tobias CW (eds) Advances in electrochemical science and engineering, chap 4, vol 5. Wiley-VCH, Weinheim
8. Prakash J, Tryk DA, Aldred W, Yeager EB (1999) J Appl Electrochem 29:1463
9. Gojković S Lj, Gupta S, Sanivell RF (1999) Electrochim Acta 45:889
10. Jiang R, Chu D (2000) J Electrochem Soc 147:4605
11. Cote R, Laland G, Faubert G, Guay D, Dodelet JP, Denes G (1998) J New Mater Electrochem Syst 1:7
12. Ranhotra GS, Haddix GW, Bell AT, Reimer JA (1987) J Catal 108:24
13. Lee JS, Oyama ST, Boudart M (1990) J Catal 125:157
14. Ledoux MJ, Pham-Huu C, Guille J, Dunlop H (1992) J Catal 134:383
15. Hyeon T, Fang M, Suslick KS (1996) J Am Chem Soc 118:5493
16. Meng H, Shen PK (2006) Electrochem Commun 8:588
17. Yang XG, Wang CY (2005) Appl Phys Lett 86:224104
18. Ganesan R, Lee JS (2005) Angew Chem Int Ed 44:6557
19. Wang SJ, Chen CH, Chang SC, Uang KM, Juan CP, Cheng HC (2004) Appl Phys Lett 85:20
20. Pinheiro ALN, Oliveira-Neto A, de Souza EC, Perez J, Paganin VA, Ticianelli EA, Gonzalez ER (2003) J New Mater Electrochem Syst 6:1
21. West AR (1984) Solid state chemistry and its applications. Wiley, New York
22. Paulus UA, Schmidt TJ, Gasteiger HA, Behm RJ (2001) J Electroanal Chem 495:134
23. Meng H, Shen PK (2005) J Phys Chem B 109:22705
24. Paulus UA, Wokaum A, Scherer GG, Schmidt TJ, Stamenkovic V, Markovic NM, Ross PN (2002) Electrochim Acta 47:3787
25. Yang H, Vogel W, Lamy C, Alonso-Vante N (2004) J Phys Chem B 108:11024
26. Mo Y, Sarangapani S, Lê A, Scherson DA (2002) J Electroanal Chem 35:538–539
27. Pereira LGS, Santos FR, Pereira ME, Paganin VA, Ticianelli EA (2006) Electrochim Acta 51:4061
28. Lee K, Ishihara A, Mitsushima S, Kamiya N, Ota K (2004) Electrochim Acta 49:3479
29. Antoine O, Durand R (2000) J Appl Electrochem 30:839
30. Murthi VS, Urian RC, Mukerjee S (2004) J Phys Chem B 108:11011
31. Nie M, Shen PK, Wu M, Wei Z, Meng H (2006) J Power Sources 162:173
32. Toda T, Igarashi H, Watanabe M (1999) J Electroanal Chem 460:258
33. Min M, Cho J, Cho K, Kim H (2000) Electrochim Acta 45:4211
34. Bard AJ, Faulkner LR (1980) In: Electrochemical methods. Wiley, New York, p 283
35. De Melo RMQ, Ticianelli EA (1996) Electrochim Acta 42:1031
36. Breiter MW (1969) Electrochemical processes in fuel cells. Springer, New York
37. Conway BE (1965) Theory and principles of electrode processes. The Ronald Press Company, New York
38. Harrison JA, Khan ZA (1971) J Electroanal Chem 30:327